

**Simulating the deteriorating effect of the alkali-silica reaction in concrete via a micro-poro fracture mechanical model**

Esposito, R; Hendriks, MAN

**DOI**

[10.1061/9780784479346.015](https://doi.org/10.1061/9780784479346.015)

**Publication date**

2015

**Document Version**

Accepted author manuscript

**Published in**

Proceedings of the 10th international conference on mechanics and physics of creep, shrinkage, and durability of concrete and concrete structures

**Citation (APA)**

Esposito, R., & Hendriks, MAN. (2015). Simulating the deteriorating effect of the alkali-silica reaction in concrete via a micro-poro fracture mechanical model. In C. Hellmich, B. Pichler, & J. Kollegger (Eds.), *Proceedings of the 10th international conference on mechanics and physics of creep, shrinkage, and durability of concrete and concrete structures* (pp. 118-127). American society of civil engineers. <https://doi.org/10.1061/9780784479346.015>

**Important note**

To cite this publication, please use the final published version (if applicable). Please check the document version above.

**Copyright**

Other than for strictly personal use, it is not permitted to download, forward or distribute the text or part of it, without the consent of the author(s) and/or copyright holder(s), unless the work is under an open content license such as Creative Commons.

**Takedown policy**

Please contact us and provide details if you believe this document breaches copyrights. We will remove access to the work immediately and investigate your claim.

# INFLUENCE OF THE ALKALI-SILICA REACTION ON THE MECHANICAL DEGRADATION OF CONCRETE

Rita Esposito,<sup>1</sup> Caner Anaç,<sup>2</sup> Max A.N. Hendriks,<sup>3 4</sup> and Oğuzhan Çopuroğlu<sup>5</sup>

## 1 Abstract

2 The alkali-silica reaction (ASR) is an important problem that has yet to be completely under-  
3 stood. Due to the complexity of this phenomenon, a number of studies have been conducted to  
4 characterize its kinetics, its impact on the material and its structural consequences. This paper fo-  
5 cuses on the deteriorating impact of ASR on concrete material, not only in terms of concrete swell-  
6 ing but also in consideration of the induced mechanical degradation. The relationships between  
7 concrete expansion and various engineering properties, which are key parameters in structural as-  
8 sessments, are investigated. First, new mechanical test results are presented. Second, available  
9 literature data on the evolution of engineering properties of ASR-affected concrete under free-  
10 expansion conditions, are collected and statistically analysed. The elastic modulus was found to  
11 be the best indicator for identifying the progression of ASR in concrete. Conversely, the evolution  
12 of compressive strength was observed to potentially mask damage resulting from the ASR. The  
13 tensile behaviour of affected concrete was better represented by the splitting tensile test.

14 **Keywords:** Alkali-silica reaction (ASR), Damage assessment, Degradation, Mechanical proper-  
15 ties

## 16 INTRODUCTION

---

<sup>1</sup>Ph.D. Candidate, Dept. of Structural Engineering, Delft University of Technology, Stevinweg 1, 2628CN, Delft, The Netherlands. E-mail: r.esposito@tudelft.nl.

<sup>2</sup>Ph.D. Candidate, Dept. of Structural Engineering, Delft University of Technology, Stevinweg 1, 2628CN, Delft, The Netherlands. E-mail: c.anac@tudelft.nl.

<sup>3</sup>Associate professor, Dept. of Structural Engineering, Delft University of Technology, Stevinweg 1, 2628CN, Delft, The Netherlands. E-mail: m.a.n.hendriks@tudelft.nl.

<sup>4</sup>Professor, Dept. of Structural Engineering, Norwegian University of Sciences and Technology (NTNU), Richard Birkelands vei 1a, 7491, Trondheim, Norway.

<sup>5</sup>Assistant professor, Dept. of Structural Engineering, Delft University of Technology, Stevinweg 1, 2628CN, Delft, The Netherlands. E-mail: o.copuroglu@tudelft.nl.

17 Because the service life design of concrete structures has become an important topic in con-  
18 struction projects, considerations of durability issues are being included in the design phase. In this  
19 group, the alkali-silica reaction (ASR) is known for its complex chemistry and physical mechan-  
20 isms, which makes predicting the behaviour of ASR-affected concrete structures very challenging.

21 Various investigations regarding the structural effects of the ASR have been conducted over  
22 the past decade. Attention has particularly been focussed on infrastructures such as hydroelectric  
23 power plants and bridges. The first studies were performed on dams and accompanied by struc-  
24 tural analyses (Léger et al. 1996; Malla and Wieland 1999; Huang and Pietruszczak 1999; Ulm  
25 et al. 2000; Capra and Sellier 2003; Li and Coussy 2004; Saouma et al. 2007; Comi et al. 2009;  
26 Saouma 2013), along with the development of the first engineering models concerning ASR. Later,  
27 structural effects of the ASR on concrete members were investigated under laboratory conditions,  
28 primarily using shear and flexural tests on beams (Fan and Hanson 1998; Clayton et al. 1990; den  
29 Uijl 2002; Multon 2004; Inoue et al. 2012; Martin et al. 2012; Mikata et al. 2012; Miyagawa et al.  
30 2012; Ramezani-pour and Hajighasemali 2012). Meanwhile, the framework was narrowed to  
31 investigate the anisotropic expansion behaviour induced by the coupling between expansive alkali-  
32 silicate gel, material expansion and external mechanical loading (Larive 1998; Multon 2004).

33 Various experimental campaigns also studied the degradation of mechanical properties induced  
34 by gel expansion in laboratory samples stored under free-expansion conditions (Swamy and Al-  
35 Asali 1988; Larive 1998; Ahmed et al. 2003; Monette 1997; Multon 2004; Ben Haha 2006; Giaccio  
36 et al. 2008; Sargolzahi et al. 2010; Giannini and Folliard 2012; Lindgård 2013; Sanchez et al. 2014)  
37 The experimental focus was on the compressive strength, which is the most widely used material  
38 parameter in structural assessments. The results were contradictory and a clear degradation trend  
39 for the compressive strength could not be identified. Conversely, the elastic modulus was always  
40 found to be sensitive to the reaction.

## 41 **RESEARCH SIGNIFICANCE**

42 By considering a wider scope of structural assessments, this paper aims to highlight the im-  
43 portance of mechanical degradation in relation to ASR-induced concrete expansion. In current

44 practice, the ASR reactivity of a concrete mix is evaluated through accelerated laboratory tests  
45 on unconstrained samples. However, the results from these tests do not directly relate to the real  
46 performance of concrete within a structure. The performance of concrete is generally expressed in  
47 terms of expansion and expansion rates, which can considerably differ substantially for different  
48 concrete mixes and environmental conditions (Larive 1998; Lindgård 2013). Here the observed  
49 expansion and expansion rates were considered as given. The specific goal was to find a trend  
50 between the deterioration of the mechanical properties and the observed swelling of concrete un-  
51 der free-expansion conditions regardless of the wide variety of concrete mixes used and the exper-  
52 imental conditions applied.

53 First, the experimental results obtained by the authors are presented. The classification and  
54 normalisation procedures are described as an introduction to the following statistical analysis.  
55 Second, available literature data on the mechanical degradation of ASR-affected concrete under  
56 free-expansion conditions are summarised. The relation between ASR-induced expansion and the  
57 mechanical degradation of concrete is statistically analysed.

## 58 **EXPERIMENTAL RESEARCH**

59 In 2010 a large experimental campaign was begun at the Delft University of Technology (TU  
60 Delft) under the framework of the PAT-ASR project (Performance Assessment Tool for Alkali-  
61 Silica Reaction) (Anaç et al. 2012). The scope of this research was to investigate the damage  
62 effects induced by the ASR in concrete on various scales: from microscopic to macroscopic scale.

63 In this section, the results for the macroscopic scale on the deteriorating impact of ASR on  
64 concrete in terms of expansion and the degradation of mechanical properties are reported. The  
65 experimental results are evaluated in a statistical context through the introduction of a classification  
66 and a normalisation procedure. Each concrete mix is classified on the basis of the expansion value  
67 obtained in a in prescribed testing duration. Their mechanical properties are normalised to identify  
68 a degradation trend.

## 69 **Materials and test methods**

70 Two comparable concrete mixes were adopted throughout this study using Dutch and Norwe-  
71 gian aggregates. The latter represents the concrete mix used in the Nautesund bridge (Norway),  
72 which exhibited severe ASR damage. The Nautesund bridge is a unique case, because from con-  
73 struction to demolition, all materials and structural details were properly documented. Through a  
74 collaboration between the Delft University of Technology (TU Delft) and the Norwegian Roads  
75 Public Administration (NPRA), concrete samples of this structure were used in the PAT-ASR pro-  
76 ject for verification purposes.

77 Concrete mixes cast with Dutch and Norwegian aggregates are respectively classified as RR1  
78 and RR2 mixes, as clarified in the next subsection. Norwegian aggregates in the RR2 mix were  
79 primarily composed of coarse-grained quartz, quartzite, gneiss, metarhyolite and other minor rock  
80 types. By implementing the point count method, it was estimated that 33% of aggregates with  
81 a size of 0-8 mm and 36% of coarse gravel were potentially alkali-reactive. Dutch aggregates  
82 in the RR1 mix were primarily composed of quartzite, quartz, (calcareous) chert, volcanic rock  
83 fragments and other minor rock types. Thus far no alkali reactivity has been reported for these  
84 aggregates. The adopted mix proportions of cement/fine aggregates/coarse aggregates/water were  
85 1:2.93:1.68:0.46 for the RR1 mix and 1:3.03:1.74:0.45 for the RR2 mix by weight. NORCEM  
86 Industri (CEM I 42.5R) cement with a dosage of 380 kg/m<sup>3</sup> and an equivalent Na<sub>2</sub>O<sub>eq</sub> content  
87 of 1.17% was used. The two concrete mixes were designed to have a similar aggregate gradation  
88 and a comparable 28-day compressive strength. Therefore, to properly define the mix design, the  
89 density, the apparent specific gravity (ASG), the water absorption and the moisture of aggregates  
90 were identified following ASTM C127 (2012a) and ASTM C128 (2012b). Tables 1 and 2 list the  
91 characteristics of the concrete mixes and cement, respectively.

92 Due to the large number of samples needed, they were cast in six sessions; in each session,  
93 control casting cubes, which were not subjected to ASR treatment, were prepared. Table 3 lists  
94 the concrete properties for each cast. Cube specimens with sides of 150 mm were stored for 28  
95 days at 20 °C in a fog room and subsequently tested under uniaxial compression loading following

96 NEN-EN 12390-3:2002 (2002). The load was applied at a constant rate of 0.60 MPa/s. In order  
97 to determine the evolution of the mechanical properties of ASR affected concrete, expansion and  
98 mechanical tests were performed on prisms and cubes stored at 38 °C and a relative humidity of  
99 greater than 96% (RILEM TC 219-ACS Alkali-Silica Reaction in Concrete Structures 2011). An  
100 overview of the storage conditions and sample sizes is given in Table 4. The samples were placed  
101 on top of a metallic grid in plastic boxes; 2 cm of water at the bottom of the box ensured high  
102 humidity. The plastic boxes were placed in custom plastic reactors containing water, in which the  
103 plastic boxes were immersed 10 cm in water. The reactors included built-in heating elements to  
104 heat the water. During the storage period temperature sensors were placed inside the boxes and  
105 in the reactors to control the temperature, whereas humidity sensors were installed only in the  
106 reactors. The samples were tested at 14, 28, 49, 91, 182, 252 and 365 days.

107 The expansion values were measured on 75x75x280-mm prisms according to the procedure  
108 proposed by RILEM recommendation AAR-3 (2011). Tests for determining the static elastic  
109 modulus were performed on 100x100x400-mm prisms in agreement with ISO 1920-10:2010(E)  
110 (2010). Linear Variable Differential Transformers (LVDTs) were employed to measure vertical and  
111 horizontal displacements. The vertical LVDTs were centrally placed on each side of the sample  
112 over a length of 200 mm. The alternative method was selected, in which the strain and stress on  
113 the test specimen were continuously measured during the loading cycle. First, a basic stress of  
114 0.50 MPa was applied for 60 s; afterwards, the strain was constantly increased until the peak was  
115 reached. The static elastic modulus  $E_{st}$  and the Poisson ratio  $\nu$  were determined in the elastic  
116 phase of the curve, between the basic stress level and one third of the peak stress. The peak stress  
117 was chosen as a measure of the compressive strength  $f_c$ . The splitting tensile strength  $f_{t,sp}$  was  
118 measured for cubes with sides of 150 mm, which is in agreement with EN 13290-6:2009 (2009).  
119 The load was applied with a constant increase of 0.05 MPa/s.

## 120 **Results**

121 Table 5 lists the results from the expansion and the mechanical tests for both mixes. Each result  
122 was determined as the average of three measurements performed on samples of the same cast. The

123 number of the cast from which each set of three samples was prepared is listed, thereby making a  
124 distinction between samples employed for the expansion and mechanical tests (e.g., 4 - 1 means  
125 that the expansion measurements were performed on samples prepared in cast number 4, while the  
126 corresponding mechanical tests refer to samples prepared in cast number 1). The mix design, the  
127 properties of fresh concrete and the 28-day cubic compressive strength of each cast are presented  
128 in Tables 1 and 3. The coefficients of variation of 28-day cubic compressive strength for the RR1  
129 and RR2 concrete mixes were found to be 5.1 and 4.4%, respectively.

130 The asymptotic expansion obtained after one year was 0.11% for the RR1 mix and 0.18% for  
131 the RR2 mix (Figure 1(a)). Both mixes appeared reactive according to the RILEM recommend-  
132 ation AAR-0 (2012) and exceeded the recommendation expansion threshold values of 0.05 and  
133 0.1%. The classification proposed by RILEM recommendation AAR-0 (2012) has been extended  
134 and further applied in the next section. Three classes of mixes were defined on the basis of the  
135 maximum concrete expansion reached within the testing time. The concrete mixes were classified  
136 as potentially reactive mixes (PR) if their expansion was  $0.05\% \leq \varepsilon \leq 0.10\%$ , or as reactive mixes  
137 (RR) if their expansion was  $0.10\% < \varepsilon < 0.50\%$ , or as extremely reactive mixes (ER) if their  
138 expansion was greater than 0.50%. If the concrete expansion was found to be  $\varepsilon \leq 0.05\%$ , the mix  
139 was considered to be non-reactive.

140 In Figure 1(b)-d, the degradation of the mechanical properties is reported in terms of normalised  
141 values versus expansion. Each normalised value  $\beta_P$  was obtained as the ratio between the current  
142 property value  $P$  and its reference one  $P^{\text{ref}}$ . The latter was estimated at a reference expansion  
143 of 0.05%, which is the value used to discriminate between non-reactive and potentially reactive  
144 concrete. This normalisation procedure is also adopted in the next section, in which available  
145 literature data are compared and analysed to describe the degradation behaviour.

146 The mechanical properties exhibited a slight increase during the first 90 days, followed by a  
147 degradation trend. The static elastic modulus (Figure 1(b)) of concrete mix RR1 exhibited minor  
148 variations and ranged between 99 and 107% of its reference value. Conversely, the concrete mix  
149 RR2 exhibited a maximum degradation of 35%. The normalised compressive strength (Figure

150 1(c)) exhibited a pronounced initial increase from 0.76 to 0.90 for RR1 concrete and from 0.88 to  
151 0.97 for RR2 concrete. After both concrete mixes tend to the asymptotic value of 1. The splitting  
152 tensile strength (Figure 1(d)) reported a similar trend for both mixes. After a relatively small initial  
153 increment a degradation was observed, which obtained a maximum value of 23% for concrete mix  
154 RR1 and of 26% for concrete mix RR2.

155 In conclusion, the studied RR1 and RR2 mixes were both classified as reactive, which is in  
156 agreement with the proposed classification procedure. The RR2 concrete presented highest expan-  
157 sion, and it showed a relevant degradation in terms of its static elastic modulus and splitting tensile  
158 strength. The RR1 concrete, which presented lower expansion, showed a constant tendency for  
159 the static elastic modulus; however, its deterioration in terms of splitting tensile strength follows  
160 the same trend as that for the RR2 concrete. Both concrete mixes showed an initial increase in  
161 compressive strength, which was followed by a nearly constant progression when the reference  
162 value was approached.

## 163 **STUDY OF THE MECHANICAL DEGRADATION INDUCED BY THE ALKALI-SILICA** 164 **REACTION**

165 To study the degradation of mechanical properties induced by the alkali-silica reaction, avail-  
166 able literature experimental data were collected, along with the data presented in the previous  
167 section. A statistical analysis was performed to determine trends in the degradation behaviour.

### 168 **Overview of literature data**

169 Over the past 30 years, various authors have tested the degradation of mechanical properties  
170 induced by ASR in concrete samples stored under free-expansion conditions. In this overview  
171 the results obtained by Swamy et al. (1988), Larive (1998), Ahmed et al. (2003), Monette et al.  
172 (1997), Multon (2004), Ben Haha (2006), Giaccio et al. (2008), Sargolzahi et al. (2010), Giannini  
173 and Folliard (2012), Lindgård (2013) and Sanchez et al. (2014), as well as the results presented  
174 earlier in this paper are used.

175 Tables 6 and 7 list the concrete properties and storage conditions employed by the various  
176 authors. A variety of natural aggregates was used. In a few cases (Swamy and Ahmed) non-natural

177 aggregates were adopted to accelerate the reaction. This practice, although often criticised, is still  
178 sometimes used to understand the ASR mechanism in concrete (Bažant et al. 2000). The water-  
179 to-cement ratio, W/C, chosen in these studies varied between 0.30 and 0.61, and the equivalent  
180 alkali content ranged between 0.40 and 2.25%. The majority of the authors stored their samples at  
181 38 °C ( $\pm 2$  °C), ensuring a high relative humidity or placing the samples in water. These storage  
182 conditions are now prescribed by current standards and recommendations (e.g., ASTM C1293  
183 (2001) and RILEM recommendation AAR-3 (2011)). In general, the samples were not wrapped  
184 and stored in plastic or metal boxes. Pre-treatment was applied by 6 of 12 authors, who primarily  
185 kept the samples at 20 °C in fog room. The samples were demoulded after one day, with the  
186 exception of Larive, who kept the samples in moulds for three days.

187 To analyse the data, mixes were classified on the basis of the asymptotic expansion value ob-  
188 tained within the prescribed testing time (Table 8). If a test was terminated before the prescribed  
189 testing duration had elapsed (Monette and Giannini), the asymptotic expansion was chosen at the  
190 end of the test. In contrast, when the test went beyond the testing duration (Larive and Sargolzhahi),  
191 the asymptotic expansion was calculated by interpolation. In the cases where different storage  
192 conditions were used (Ben Haha and Lindgård), the asymptotic expansion was defined for the con-  
193 dition closest to the one proposed by RILEM recommendation AAR-3 (2011). The classification  
194 procedure presented in the previous section was adopted, and the concrete mixes were divided into  
195 potentially reactive (PR,  $0.05\% \leq \varepsilon \leq 0.10\%$ ), reactive (RR,  $0.10\% < \varepsilon < 0.50\%$ ) and extremely  
196 reactive (ER,  $\varepsilon \geq 0.50\%$ ). Non-reactive mixes ( $\varepsilon \leq 0.05\%$ ) were not considered. To distinguish  
197 between the different data sets, the name of the first author was indicated. If the same authors  
198 tested more than one mix in the same reactivity class, an Arabic number was added to the data set  
199 name (e.g., Swamy-ER1 and Swamy-ER2). If an author tested the same mix with different propor-  
200 tions, a Roman numeral between i and iii was added to the data set name (e.g., Ben Haha-PR1ia,  
201 Ben Haha-PR1iia and Ben Haha-PR1iiaa). If an author tested the same mix design under different  
202 storage conditions, the letters a, b and c were added to the data set name (e.g., Lindgård-PR1a,  
203 Lindgård-PR1b and Lindgård-PR1c). To compare the results, the normalisation procedure presen-

204 ted in the previous section was adopted. The reference values at an expansion of  $\varepsilon = 0.05\%$  were  
205 generally interpolated and they are listed in Table 8.

206 The majority of the authors studied the degradation of the compressive strength  $f_c$  (10 of 12  
207 authors) and of the static elastic modulus  $E_{st}$  (9 of 12 authors), as shown in Table 8. The tensile  
208 behaviour was studied by 7 of 12 authors, who preferred the use of the splitting tensile strength  
209  $f_{t,sp}$  above the modulus of rupture MOR and the direct tensile strength  $f_{t,dir}$ . Non-destructive tests  
210 for determining the dynamic elastic modulus  $E_{dyn}$  were chosen by 5 of 12 authors.

211 Figures 2 and 3 report the variations in the mechanical properties as functions of the con-  
212 crete expansion. Four zones were defined: the low-expansion zone ( $\varepsilon < 0.05\%$ ), the moderate-  
213 expansion zone ( $0.05\% \leq \varepsilon \leq 0.10\%$ ), the high-expansion zone ( $0.10\% < \varepsilon < 0.50\%$ ) and the  
214 extreme-expansion zone ( $\varepsilon \geq 0.50\%$ ). Each data point is an average of the results obtained from  
215 testing three samples, with the exception of Swamy, who adopted two samples. For clarity, the  
216 figures employ a non-uniformly scaled expansion axis and the legend is reported in Table 8. Fig-  
217 ures 4 and 5, which will be discussed in the next subsection, show the data with a uniformly scaled  
218 expansion axis.

219 It was found that the elastic modulus is subjected to a significant degradation (Figures 2(a) and  
220 2(b)). Both the static and dynamic elastic moduli marginally increase for expansion values up to  
221 0.03%. Subsequently, a slight degradation is observed in the low- and moderate-expansion zones;  
222 however their mean values remain close to unity in these zones. For expansion values greater than  
223 0.10%, both of the stiffness properties decreased at similar rate. The maximum degradation was  
224 obtained in the extreme-expansion zone, with a reduction of 92% for the static elastic modulus  
225 and of 86% for the dynamic one. The non-destructive test provided a more dense data cluster with  
226 respect to the destructive test.

227 The compressive strength was extensively investigated by many authors, although Swamy and  
228 Al-Asali stated in 1988, *ipse dixit* "compressive strength is not a good indicator of the initiation or  
229 progress of ASR". Figure 2(c) confirms this tendency. In the low-expansion zone, the normalised  
230 value of compressive strength ranged between 0.59 and 1.62, with an average of 0.92. The data

231 sets that obtained the lowest and highest normalised compressive strength values are the mixes  
232 PR1ia and PR2ia, respectively, (both tested by Ben Haha (2006)), which contained the lowest  
233 alkali content ( $N_{a_2O_{eq}} = 0.4\%$ ) and were stored at a temperature of 20 °C under high humidity.  
234 Due to the low alkali content and the non-accelerated storage conditions, it can be hypothesised  
235 that the ASR did not lead to a significant concrete expansion and that the increase in strength can  
236 be attributed to the hydration process. Excluding these data sets, the maximum normalised value in  
237 the low-expansion zone equals 1.04. In the moderate-expansion zone, the data cluster narrows, and  
238 the normalised value of the compressive strength increases to 1.28. For expansion values greater  
239 than 0.15% the majority of the concrete mixes exhibit a degradation in term of strength; however,  
240 the data show a substantial number of exceptions. The maximum degradation is obtained in the  
241 extreme-expansion zone, with a reduction of 46%.

242 The tensile behaviour of ASR-affected concrete (Figure 3) was found to be sensitive to the test  
243 method, as previously observed for unaffected concrete. Whereas the splitting (Figure 3(a)) and  
244 flexural (Figure 3(b)) tests show an important decrease in the strength for high-expansion values,  
245 the direct tensile strength (Figure 3(c)) appears to be less sensitive. In the low-expansion zone, the  
246 normalised values of all three tensile strengths are close to unity. After the data clusters spread out,  
247 and both the splitting tensile strength and the modulus of rupture drastically decrease. The direct  
248 tensile strength exhibits a relevant degradation only in the extreme-expansion zone. However, the  
249 data are limited to only three concrete mixes tested by the same author (Ahmed et al. 2003), which  
250 are classified as reactive and extremely reactive. The few data points are spread over an expansion  
251 scale that ranges between -0.03 and 2.70%; therefore, a detailed picture of the degradation trend is  
252 missing, which can strongly influence the estimation of the reference values. The three strengths  
253 exhibit a maximum degradation in the extreme-expansion zone, with a reduction of 53% for the  
254 splitting tensile strength (Figure 3(a)), 89% for the modulus of rupture (Figure 3(b)), and 38% for  
255 the direct tensile strength (Figure 3(c)).

## 256 Statistical analysis

257 To determine the degradation behaviour of the mechanical properties induced by the alkali-  
258 silica reaction in free-expansion samples, a statistical analysis was performed. The normalised  
259 data were fitted on the basis of two formulations: an S-shaped curve and a piecewise linear curve.  
260 The four zones (low-, moderate-, high- and extreme-expansion zones) were considered to define  
261 the weights of each data point. Within each zone data points have the same weight, whereas the  
262 sum of the weights for each zone is equal within a weighted least squares fitting process. In this  
263 way a bias resulting from an unequal distribution of data points along the expansion axis is limited.

264 The S-shaped curve is a revised version of the degradation law proposed by Saouma and Perotti  
265 (2006) and expresses the normalised value of each property  $\beta_P$  as a function of the expansion  $\varepsilon$ ,  
266 whereby four parameters are employed:

$$\beta_P = \frac{P}{P^{\text{ref}}} = \beta_0 - (\beta_0 - \beta_\infty) \frac{1 - \exp\left(-\frac{\varepsilon}{\varepsilon_c}\right)}{1 + \exp\left(-\frac{\varepsilon - \varepsilon_1}{\varepsilon_c}\right)} \quad (1)$$

267 where  $P$  and  $P^{\text{ref}}$  are the current and reference values of the chosen property, respectively;  $\beta_0$   
268 and  $\beta_\infty$  are the normalised property values at zero expansion and at the asymptotic expansion,  
269 respectively; and  $\varepsilon_1$  and  $\varepsilon_c$  are the latency and characteristic expansion values, respectively. The  
270 latency expansion  $\varepsilon_1$  defines the delay before a relevant degradation of the mechanical property is  
271 observed: the lower the latency expansion, the earlier the degradation is observed. The charac-  
272 teristic expansion  $\varepsilon_c$  contributes to the degradation rate, which is defined as the average decrease  
273 between  $\varepsilon_1$  and  $\varepsilon_1 + 2\varepsilon_c$ .

274 Figure 4 shows the resulting S-shaped curves along with the experimental data. The fitting coeffi-  
275 cients and the estimation errors, in terms of standard deviation, are reported in Table 9.

276 In Figure 4(a) the elastic modulus data are denoted by grey dots for destructive tests and by white  
277 dots for non-destructive tests. The fitting was formulated by considering all the data (thick continu-  
278 ous line) or by distinguishing between static (thick dash-dot line) and dynamic (thin continuous  
279 line) elastic modulus data. The curves exhibit a minor difference only in the extreme-expansion

280 zone. Therefore, all the data can be considered to be representative of the stiffness degradation in  
281 concrete subjected to the ASR. The estimation error is 7%. The resulting latency time  $\varepsilon_1$  is ex-  
282 tremely small (on the order of  $10^{-14}$ ), which confirms the fast stiffness degradation starting in the  
283 low-expansion zone. The maximum,  $\beta_0$ , and the minimum,  $\beta_\infty$ , normalised values of the elastic  
284 modulus equal 1.06 and 0.19.

285 Figure 4(b) shows the degradation S-shaped curve for the compressive strength. Due to the nature  
286 of the formulation, the initial increase in strength cannot be captured; as a result the maximum  
287 normalised value  $\beta_0$  is equal to 1.00 and the latency expansion  $\varepsilon_1$  is 0.51%. The S-shaped curve  
288 exhibits an asymptote at 0.64. The estimation error is 15%.

289 In Figure 4(c), the tensile strength data are denoted by grey, white and black dots to indicate the  
290 splitting, flexural and direct tensile tests, respectively. The fitting was formulated by considering  
291 all the data (thick continuous line) or by distinguishing between the three test methods. As previ-  
292 ously mentioned, the test type has a strong influence on the resulting strength. Consequently, it is  
293 more appropriate to consider each test method separately. The curve based on the splitting tensile  
294 strength data (thick dash-dot line) provides the best fitting with an error of 8%. Its normalised value  
295 can range between 1.01 and 0.60. The degradation becomes pronounced after a latency expansion  
296  $\varepsilon_1$  of 0.35%. The modulus of rupture (thin continuous line) begins to degrade at approximately the  
297 same expansion level ( $\varepsilon_1 = 0.37\%$ ); it can reach a maximum deterioration of 76%. The estimation  
298 error is 20%, which is relatively high. The direct tensile strength (thin dash-dot line) exhibits a  
299 maximum degradation of 30%. The degradation starts at a latency expansion  $\varepsilon_1$  of 2.15%, meaning  
300 that the fitting mainly follows the behaviour of the concrete mix Ahmed-ER2. The estimation error  
301 is 12%.

302 The statistical analysis was extended by considering a continuous piecewise linear function.  
303 This choice was made to allow for an increase in the mechanical properties, e.g., as observed  
304 for the compressive strength. The continuity points are represented by the expansion values that  
305 delimit the four zones; the formulation is as follows:

$$\beta_P = \frac{P}{P^{\text{ref}}} = \begin{cases} q_l + m_l \varepsilon & \varepsilon \leq 0.05\% \\ q_m + m_m \varepsilon & 0.05\% < \varepsilon \leq 0.1\% \\ q_h + m_h \varepsilon & 0.1\% < \varepsilon \leq 0.5\% \\ q_e + m_e \varepsilon & \varepsilon > 0.5\% \end{cases} \quad (2)$$

306 where  $q$  and  $m$  the linear coefficients for each zone. Due to the continuity condition, the number  
 307 of unknown coefficients reduces to five; three of the coefficients can be determined as follows:

$$q_m = q_l + (m_l - m_m) 0.05; \quad q_h = q_m + (m_m - m_h) 0.1; \quad q_e = q_h + (m_h - m_e) 0.5 \quad (3)$$

308 Figure 5 shows the resulting piecewise linear curve along with the experimental data. The fitting  
 309 coefficients and the estimation errors, in terms of standard deviation, are reported in Table 9.

310 The elastic modulus degradation (Figure 5(a)) was well described by the piecewise linear curve.  
 311 The estimation error and the degradation rate, which were evaluated in the high-expansion zone,  
 312 provide results that are similar to those obtained from the S-shaped curve fitting. For expansion  
 313 values greater than 2.60% this formulation provides unrealistic negative normalised values for the  
 314 elastic modulus; therefore, zero residual stiffness should be considered after this limit.

315 The piecewise linear curve better described the behaviour of the compressive strength (Figure  
 316 5(b)), which shows an increase in the moderate-expansion zone. The total estimation error is  
 317 slightly decreased to 13%. However, considering the moderate-expansion zone only, the estimation  
 318 error is reduced from 20 to 13%.

319 The piecewise linear curve exhibited similar trend and estimation error with respect to the S-shaped  
 320 curve for the splitting tensile strength (Figure 5(c)). This formulation is able to capture the slight  
 321 increase in strength observed for the modulus of rupture in the moderate-expansion zone.

322 In Figure 6(a), the best curve fitting results are presented along with an error band equal to  $2\sigma$ .  
 323 The piecewise linear curve was chosen to describe the compressive strength behaviour, whereas  
 324 the S-shaped curve was chosen to describe the other properties. The tensile strength behaviour  
 325 has been reported in terms of the splitting test results. Both static and dynamic elastic modulus

326 data were considered for describing the stiffness degradation. According to the curve fitting stud-  
327 ies, the elastic modulus was found to be the best indicator of ASR signs in concrete. The data  
328 show a relevant degradation, already at early expansion, which is characterized by the highest  
329 rate. For high-expansion values ( $\varepsilon > 2.00\%$ ) the residual stiffness is 20% of the reference value.  
330 Conversely, the compressive strength behaviour is described with an initial gain of 15% and a max-  
331 imum reduction of 46%. However, the estimation error is high, approximately 13%. The tensile  
332 behaviour appears to be well described by the splitting test results. In the high-expansion zone the  
333 tensile strength degrades at a similar rate as the elastic modulus, but its deterioration is delayed.  
334 The residual value is 46%.

335 Alternately, Figure 6(b) shows the differences in degradation behaviour from comparing the  
336 stiffness and strength properties. When the elastic modulus reaches 85% of its original value,  
337 both strengths decrease at a similar rate but still slower than the degradation rate of the elastic  
338 modulus. At a normalised value of  $\beta_E = 0.50$  for the elastic modulus, the normalised splitting  
339 strength obtains an asymptotic value of  $\beta_{f_{t,sp}} = 0.60$ . The compressive strength experiences a  
340 drastic deterioration to a normalised value of the elastic modulus of  $\beta_E = 0.20$ .

341 In engineering, it is common practice to express the stiffness  $E$  and tensile strength  $f_t$  of  
342 unaffected concrete as a function of its compressive strength  $f_c$ . Using the strength-stiffness rela-  
343 tionships proposed by Model Code 2010 (CEB-FIP 2011), the degradation rate of the compressive  
344 and tensile strength of unaffected concrete shown to be lower than that for the elastic modulus  
345 (Figure 6(b)). To demonstrate this, ASR-affected concrete with a compressive strength reduction  
346 of 20% ( $\beta_{f_c} = 0.80$ ) is considered. Adopting the Model Code formulation, the estimated normal-  
347 ised values of the elastic modulus and tensile strength are 0.94 and 0.86, respectively. Considering  
348 the proposed curves, the degradation of the stiffness and tensile strength are substantially different;  
349 the normalised values are  $\beta_E = 0.35$  and  $\beta_{f_{t,sp}} = 0.60$ . This demonstrates that for ASR-affected  
350 concrete, the engineering strength-stiffness relationships cannot be used to determine the elastic  
351 modulus and the tensile strength from the measured compressive strength.

## 352 CONCLUDING REMARKS

353 The alkali-silica reaction is a harmful degradation process that can compromise the durability  
354 and serviceability of concrete structures. From investigations on structures and concrete members  
355 down to the microscopic level, numerous researchers have attempted to describe the structural con-  
356 sequences of ASR-induced concrete expansion with varying success. Although a literature survey  
357 shows that there is a strong coupling between concrete swelling and the degradation of mechanical  
358 properties, numerous findings have never led to a widely agreed upon picture. This paper attempted  
359 to clarify the relationship between concrete expansion due to the ASR and consequent degradation  
360 (or enhancement) of engineering properties.

361 First, the laboratory tests performed by the authors were presented. The authors investigated  
362 the evolution of the static elastic modulus, compressive strength and splitting tensile strength in  
363 two comparable reactive concrete mixes composed of Dutch and Norwegian aggregates. These  
364 tests belong to an extensive research project that aims to study the ASR degradation effects on  
365 various scales, from micro to macro, in order to better understand the phenomenon.

366 Second, available literature data, which focus on the evolution of engineering properties of  
367 ASR-affected concrete under free-expansion conditions, were collected and statistically analysed.  
368 When expressing the data as a function of the concrete expansion, a clear trend could be observed.  
369 The data were categorised into four reactivity classes: non-reactive ( $\varepsilon < 0.05\%$ ), potentially react-  
370 ive ( $0.05\% \leq \varepsilon \leq 0.10\%$ ), reactive ( $0.10\% < \varepsilon < 0.50\%$ ) and extremely reactive ( $\varepsilon \geq 0.50\%$ ).  
371 A normalisation procedure was adopted: each normalised value was obtained as the ratio between  
372 the current value of the property and its (calculated) reference value, which corresponds to an ex-  
373 pansion of 0.05%. The statistical analysis considered two fitting laws: an S-shaped curve and an  
374 piecewise linear curve.

375 The elastic modulus was identified as the best indicator of ASR signs in concrete, showing  
376 relevant degradation already at small expansion values. A deterioration of up to 90% could be  
377 observed. Both static and dynamic elastic modulus tests can contribute to the definition of the  
378 residual stiffness in the material. The curve fitting provides good results for both laws, with an  
379 estimation error of 7%.

380 The influence of the ASR on the compressive strength has been widely investigated. This  
381 test method is one of the principal techniques adopted in structural assessments. However, this  
382 method was determined to be the worst indicator in terms of monitoring the ASR. The compressive  
383 strength exhibits an initial gain of approximately 15% in the low- and moderate-expansion zones  
384 and a subsequent decreases to 46% of its original value. The piecewise linear curve provides the  
385 best fitting, thereby allowing the description of a non-monotonic trend. The estimation error is  
386 approximately 13%.

387 The splitting test best captured the influence of the ASR on the tensile behaviour of concrete.  
388 The data show an initial delay with respect to the degradation of the elastic modulus but a similar  
389 deterioration rate in the high-expansion zone. The splitting tensile strength eventually decreases to  
390 64%. The S-shaped curve provided the best fitting with an estimation error of 8%.

391 When comparing the degradation behaviour of compressive and splitting tensile strengths with  
392 respect to the elastic modulus, a non-linear relation was observed. Consequently, the ASR-affected  
393 concrete appears to be a substantially different material and the known engineering strength-  
394 stiffness relationships, developed for unaffected concrete, cannot be applied.

395 The correlation between mechanical degradation and concrete expansion, which appears fun-  
396 damental to the assessment of ASR-affected concrete structures, should be further investigated  
397 systematically to obtain narrowed bounds. Various parameters such as the specimen size, the stor-  
398 age conditions, the type of aggregates and the confinement of the samples, can play an important  
399 role in this phenomenon. To obtain statistically relevant data sets, additional experimental cam-  
400 paigns are necessary.

## 401 **ACKNOWLEDGEMENTS**

402 This work is part of the project "Performance Assessment Tool for Alkali-Silica Reaction"  
403 (PAT-ASR, STW grant no. 10977, <http://pat-asr.blogspot.nl/>), which is developed in the context of  
404 the IS2C program (<http://is2c.nl/>). The authors wish to express their thanks to the Dutch National  
405 Foundation (STW), the Dutch Ministry of Infrastructures and the Environment (Rijkswaterstraat),  
406 SGS and TNO DIANA BV for their financial support. The authors are grateful to the Norwegian

407 Public Roads Administration (Statens Vegvesen) and SINTEF for their collaboration.

## 408 **References**

409 Ahmed, T., Burley, E., Rigden, S., and Abu-Tair, I. (2003). “The effect of alkali reactivity on the  
410 mechanical properties of concrete.” *Construction and Building Materials*, 17(2), 123–144.

411 American Society for Testing and Materials (2001). *ASTM C1293 - Standard Test Method for De-*  
412 *termination of Length Change of Concrete Due to Alkali-Silica Reaction*. West Conshohocken,  
413 PA, United States.

414 American Society for Testing and Materials (2012a). *ASTM C127 - Standard Test Method for*  
415 *Density, Relative Density (Specific Gravity), and Absorption of Coarse Aggregate*. West Con-  
416 shohocken, PA, United States.

417 American Society for Testing and Materials (2012b). *ASTM C128 - Standard Test Method for*  
418 *Density, Relative Density (Specific Gravity), and Absorption of Fine Aggregate*. West Consho-  
419 hocken, PA, United States.

420 Anaç, C., Esposito, R., Çopuroğlu, O., Schlangen, E., and Hendriks, M. (2012). “A tool for con-  
421 crete performance assessment for ASR affected structures: an outlook.” *14th International Con-*  
422 *ference on Alkali Aggregate Reaction (ICAAR14)*, Austin, Texas.

423 Bažant, Z., Zi, G., and Meyer, C. (2000). “Fracture mechanics of ASR in concretes with waste  
424 glass particles of different sizes.” *ASCE Journal of Engineering Mechanics*, 126(3), 226–232.

425 Ben Haha, M. (2006). “Mechanical effects of alkali silica reaction in concrete studied by SEM-  
426 image analysis.” Ph.D. thesis, École Polytechnique Fédérale de Lausanne, Lausanne, Switzerland  
427 (May).

428 Capra, B. and Sellier, A. (2003). “Orthotropic modelling of alkali-aggregate reaction in concrete  
429 structures: numerical simulations.” *Mechanics of Materials*, 35(8), 817–830.

430 CEB-FIP (2011). *Model Code for Concrete Structures (MC2010)*. International Federation for  
431 Structural Concrete (fib), Lausanne, Switzerland.

432 Clayton, N., Currie, R., and Moss, R. (1990). “The effects of alkali-silica reaction on the strength  
433 of prestressed concrete beams.” *The Structural Engineer*, 68(15), 287–292.

434 Comi, C., Fedele, R., and Perego, U. (2009). "A chemo-thermo-damage model for the analysis of  
435 concrete dams affected by alkali-silica reaction." *Mechanics of Materials*, 41(3), 210–230.

436 den Uijl, J. (2002). "Structural consequences of ASR: an example on shear capacity." *Heron*, 47(2),  
437 125–139.

438 Fan, S. and Hanson, J. (1998). "Effect of alkali silica reaction expansion and cracking on structural  
439 behavior of reinforced concrete beams." *ACI Structural Journal*, 95, 498–505.

440 Giaccio, G., Zerbino, R., Ponce, J., and Batic, O. (2008). "Mechanical behavior of concretes dam-  
441 aged by alkali-silica reaction." *Cement and Concrete Research*, 38(7), 993–1004.

442 Giannini, E. and Folliard, K. (2012). "Stiffness damage and mechanical testing of cores speci-  
443 mens for the evaluation of structures affected by ASR." *14th International Conference on Alkali*  
444 *Aggregate Reaction (ICAAR14)*, Austin, Texas.

445 Huang, M. and Pietruszczak, S. (1999). "Modeling of thermomechanical effects of alkali-silica  
446 reaction." *Journal of Engineering Mechanics*, 125(4), 476–485.

447 Inoue, A., Mikata, Y., Takahashi, Y., and Inamasu, K. (2012). "Residual shear capacity of ASR  
448 damaged reinforced concrete beams with ruptured stirrups." *14th International Conference on*  
449 *Alkali Aggregate Reaction (ICAAR14)*, Austin, Texas.

450 International Organization for Standardization (2010). *ISO 1920-10:2010(E) Testing of concrete -*  
451 *Part 10: Determination of static modulus of elasticity in compression*. Geneva, Switzerland.

452 Larive, C. (1998). "Apports combinés de l'expérimentation et de la modélisation à la com-  
453 préhension de l'alcali-réaction et de ses effets mécaniques." Ph.D. thesis, École Nationale des  
454 Ponts et Chaussées, École Nationale des Ponts et Chaussées.

455 Léger, P., Côté, P., and Tinawi, R. (1996). "Finite element analysis of concrete swelling due to  
456 alkali-aggregate reactions in dams." *Computers & Structures*, 60(4), 601–611.

457 Li, K. and Coussy, O. (2004). "Numerical assessment and prediction method for the chemico-  
458 mechanical deterioration of ASR-affected concrete structures." *Canadian Journal of Civil En-*  
459 *gineering*, 31(3), 432–439.

460 Lindgård, J. (2013). "Alkali-silica reaction (ASR) - performance testing." Ph.D. thesis, Norwe-

461 gian University of Science and Technology, Norwegian University of Science and Technology  
462 (October).

463 Malla, S. and Wieland, M. (1999). “Analysis of an arch-gravity dam with a horizontal crack.”  
464 *Computers & Structures*, 72, 267–278.

465 Martin, R., Renaud, J., Multon, S., Toutlemonde, F., et al. (2012). “Structural behavior of plain and  
466 reinforced concrete beams affected by combined AAR and DEF.” *14th International Conference*  
467 *on Alkali Aggregate Reaction (ICAAR14)*, Austin, Texas.

468 Mikata, Y., Shimazu, Y., Hatano, Y., and Inoue, S. (2012). “Flexural and shear capacity of prc  
469 beams damaged by combined deterioration due to asr and corrosion.” *14th International Con-*  
470 *ference on Alkali Aggregate Reaction (ICAAR14)*, Austin, Texas.

471 Miyagawa, T., Yokoyama, T., Yonekawa, H., Mita, T., Nakamura, K., and Ookubo, T. (2012).  
472 “Strengthening effect on prestressed concrete memebtrs affected by alkali-silica reaction (ASR).”  
473 *14th International Conference on Alkali Aggregate Reaction (ICAAR14)*, Austin, Texas.

474 Monette, L. J. (1997). “Effects of the alkali-silica reaction on unloaded, statically loaded and  
475 dynamically loaded reinforced concrete beams.” M.S. thesis, University of Ottawa, Ottawa,  
476 Ontario, Canada.

477 Multon, S. (2004). “Evaluation expèrimental et thèorique des effets mècaniques de l’alcali-rèaction  
478 sur des structures modèles.” Ph.D. thesis, Université de Marne-la-Vallèe (in collaboration with  
479 LCPC-EDF), Champs sur Marne (October).

480 Nederlands Normalisatie-instituut (2002). *NEN-EN 12390-3 Testing hardened concrete - Part 3:*  
481 *Compressive strength of test specimens*. Delft, The Netherlands.

482 Nederlands Normalisatie-instituut (2009). *NEN-EN 12390-6 Testing hardened concrete - Part 6:*  
483 *Tensile splitting strength of test specimens*. Delft, The Netherlands.

484 Ramezaniapour, A. and Hajighasemali, S. (2012). “Flexural strength of ASR affected beams un-  
485 der sustained loading.” *14th International Conference on Alkali Aggregate Reaction (ICAAR14)*,  
486 Austin, Texas.

487 RILEM TC 219-ACS Alkali-Silica Reaction in Concrete Structures (2011). *RILEM Recommended*

488 *Test Method: AAR-3 - Detection of potential alkali-reactivity - 38° C test method for aggregate*  
489 *combinations using concrete prisms (Final draft)* (September).

490 RILEM TC 219-ACS Alkali-Silica Reaction in Concrete Structures (2012). *RILEM Recommended*  
491 *Test Method: AAR-0 - Outline Guide to the Use of RILEM Methods in the Assessment of the*  
492 *Alkali-Reactivity Potential of Aggregates (Final draft)* (May).

493 Sanchez, L., Fournier, B., Jolin, M., and Bastien, J. (2014). “Evaluation of the stiffness damage test  
494 (SDT) as a tool for assessing damage in concrete due to ASR: Test loading and output responses  
495 for concretes incorporating fine or coarse reactive aggregates.” *Cement and Concrete Research*,  
496 56, 213–229.

497 Saouma, V. (2013). *Numerical Modeling of AAR*. CRC Press.

498 Saouma, V. and Perotti, L. (2006). “Constitutive model for alkali-aggregate reactions.” *ACI Mater-*  
499 *ials Journal*, 103(3), 194–202.

500 Saouma, V., Perotti, L., and Shimpo, T. (2007). “Stress, analysis of concrete structures subjected  
501 to alkali-aggregate, reactions.” *ACI Structural Journal*, 104(5), 532–541.

502 Sargolzahi, M., Kodjo, S., Rivard, P., and Rhazi, J. (2010). “Effectiveness of nondestructive testing  
503 for the evaluation of alkali-silica reaction in concrete.” *Construction and Building Materials*,  
504 24(8), 1398–1403.

505 Swamy, R. and Al-Asali, M. (1988). “Engineering properties of concrete affected by alkali-silica  
506 reaction.” *ACI Materials Journal*, 85(5), 367–374.

507 Ulm, F.-J., Coussy, O., Li, K., and Larive, C. (2000). “Thermo-chemo-mechanics of ASR expan-  
508 sion in concrete structures.” *ASCE Journal of Engineering Mechanics*, 126(3), 233–242.

509 **List of Tables**

510 1 Mixture proportions. . . . . 22

511 2 Physical and chemical characteristics of the cement. . . . . 23

512 3 Concrete properties for each cast. . . . . 24

513 4 Storage conditions of RR1 and RR2 concrete samples. . . . . 25

514 5 Experimental results and calculated reference values for normalisation procedure. . 26

515 6 Overview of experimental tests in the literature: concrete properties. . . . . 27

516 7 Overview of experimental tests in the literature: storage conditions. . . . . 28

517 8 Overview of experimental tests in the literature: data name and corresponding

518 marker in figures, asymptotic expansion and calculated reference values of the

519 measured mechanical properties. . . . . 29

520 9 Fitting coefficients and standard deviation. . . . . 30

Table 1: Mixture proportions.

Material	Amount kg/m <sup>3</sup>	Density kg/m <sup>3</sup>	ASG m <sup>2</sup> /kg	Absorption %	Moisture w. %
RR1 mix (natural Dutch aggregates)					
Cement	380	3160			
Water	175				
Aggregate 0-2 mm	581	2551	5.36	0.77	0.26
Aggregate 2-4 mm	269	2551	1.95	0.77	0.26
Aggregate 4-8 mm	264	2582	0.52	0.41	0.07
Aggregate 8-16 mm	443	2598	0.31	0.23	0.04
Aggregate 16-22 mm	195	2599	0.23	0.49	0.27
RR2 mix (crushed Norwegian aggregates)					
Cement	380	3160			
Water	171				
Aggregate 0-2 mm	601	2651	5.36	0.28	0.03
Aggregate 2-4 mm	278	2651	1.95	0.28	0.03
Aggregate 4-8 mm	273	2691	0.52	0.28	0.07
Aggregate 8-16 mm	460	2718	0.31	0.12	0.06
Aggregate 16-22 mm	200	2688	0.23	0.17	0.07

Table 2: Physical and chemical characteristics of the cement.

Property	Value	Unit
Physical properties (cf. EN 196)		
Particle analysis +90 $\mu\text{m}$	0	%
Particle analysis +64 $\mu\text{m}$	0	%
Particle analysis -24 $\mu\text{m}$	88.6	%
Particle analysis -30 $\mu\text{m}$	94.3	%
Specific surface, Blaine	565	$\text{m}^2/\text{kg}$
Compressive strength at 1 d	29.7	MPa
Compressive strength at 2 d	39.0	MPa
Compressive strength at 7 d	47.9	MPa
Compressive strength at 28 d	57.0	MPa
Chemical properties (cf. EN 196-2)		
Loss on ignition (L.O.I.)	2.21	%
Free lime	2.08	%
Tot. Chloride	0.05	%
Sulphur Trioxide $\text{SO}_3$	3.34	%
Silica $\text{SiO}_2$	19.88	%
Alumina $\text{Al}_2\text{O}_3$	4.85	%
Ferric Oxide $\text{Fe}_2\text{O}_3$	3.76	%
Lime $\text{CaO}$	61.71	%
Magnesia $\text{MgO}$	2.43	%
Phosphorus Pentoxide $\text{P}_2\text{O}_5$	0.15	%
Potassium Oxide $\text{K}_2\text{O}$	1.02	%
Sodium Oxide $\text{Na}_2\text{O}$	0.50	%
Alkali $\text{Na}_2\text{O}_{\text{eq}}$	1.17	%

Table 3: Concrete properties for each cast.

Property	Unit	Value					
		1	2	3	4	5	6
Cast							
Mix		RR1	RR1	RR2	RR1	RR2	RR2
Specific weight	kg/m <sup>3</sup>	2340	2386	2389	2382	2450	2434
Air content	%	4.8	2.7	3.6	2.4	3.3	3.8
Slump H	mm	100	-	90	215	165	120
Slump d	mm	345	565	355	427.5	462.5	407.5
28-d compressive strength	MPa	60.40	67.95	62.44	62.14	68.10	61.80

Table 4: Storage conditions of RR1 and RR2 concrete samples.

Test	Unit	Expansion	Static elastic modulus Compressive strength Poisson ratio	Splitting tensile strength	Control casting
Sample size	mm	75x75x280	100x100x400	150x150x150	150x150x150
No. samples		6	42	42	18
After casting	Time	d	1	1	1
	Temp.	°C	20	20	20
	RH	%	98	98	98
Pre-treatm.	Time	d			28
	Temp.	°C	No pre-treatment	No pre-treatment	20
	RH	%			98
ASR treatm.	Time	d	365	various up to 365	No ASR treatment
	Temp.	°C	38	38	
	RH	%	96	96	
Before test	Time	h	24	> 2	> 2
	Temp.	°C	20	20	20
	RH	%	50	50	50

Table 5: Experimental results and calculated reference values for normalisation procedure.

Time d	RR1						RR2					
	Cast	$\varepsilon$ %	$E_{st}$ GPa	$\nu$	$f_c$ MPa	$f_{t,sp}$ MPa	Cast	$\varepsilon$ %	$E_{st}$ GPa	$\nu$	$f_c$ MPa	$f_{t,sp}$ MPa
14	4 - 4	-0.002	42.1	0.19	45.7	3.95	5 - 5	0.001	29.2	0.20	53.7	4.45
28	4 - 1	0.002	42.7	0.20	50.6	3.90	5 - 3	0.004	30.5	0.21	58.5	4.30
49	4 - 1	0.005	43.1	0.26	54.3	4.30	5 - 3	0.011	33.0	0.29	59.7	4.20
91	4 - 1	0.009	43.1	0.20	53.7	4.40	5 - 3	0.018	27.4	0.24	63.7	4.55
182	4 - 2	0.037	38.9	0.28	59.4	3.85	5 - 6	0.067	25.5	0.25	60.0	3.50
252	4 - 2	0.079	40.7	0.18	61.8	3.60	5 - 6	0.123	17.0	0.27	60.1	3.50
364	4 - 2	0.113	40.1	0.18	63.0	3.30	5 - 6	0.179	17.4	0.25	59.5	3.30
Calc. ref. value		0.05	39.5	0.24	60.11	3.76		0.05	26.1	0.25	61.23	3.85

Table 6: Overview of experimental tests in the literature: concrete properties.

Author	Data set	Aggregate Type	Cement	W/C	Na <sub>2</sub> O <sub>eq</sub> %		
Swamy	ER1	amorphous fused silica (fine)	520	0.44	1.00		
	ER2	Beltane opal (fine)					
Larive	RR	Tournaisis limestone (fine and coarse)	410	0.44	1.25		
Monette	RR	siliceous limestone (fine and coarse)	423	0.61	1.25		
	RR	limestone (fine and coarse)					
Ahmed	ER1	Thames Valley sand (fine) and limestone (coarse)	400	0.50	1.75		
	ER2	Thames Valley sand (fine), fused silica (fine) and limestone (coarse)					
Multon	PR	calcareous stones with siliceous inclusions	410	0.50	1.25		
Ben Haha	PR1ia-b	chlorite interleaved	-	0.46	0.40		
	PR1iia-b-c	with layers of quartz and feldspar			0.80		
	PR1iiia-b-c	(fine and coarse)			1.20		
	PR2ia-b	biotitic schist			0.40		
	PR2iia-b-c	containing phyllosilicates			0.80		
	PR2iiia-b-c	(fine and coarse)			1.20		
Giaccio	PR	granitic stone with feldspars, quartz, micas, epidote, zircon	420	0.42	1.24		
	RR1	siliceous orthoquartzite with opal, quartz, chalcedony, microcrystalline					
	RR2	opal, chalcedony					
Sargolzahi	RR	Spratt limestone	345	0.50	1.25		
Giannini	RR1	rhyolite and other volcanics (coarse)	420	0.42	1.25		
	RR2	quartz, feldspars, siliceous volcanics, chert (fine)					
Lindgård	PR1a	Ottersbo cataclasite with crypto- to microcrystalline quartz (coarse)	400	0.45	2.25		
	PR2a		550	0.30	0.67		
	RR1a		315	0.60	1.17		
	RR2a		400	0.45	0.93		
	PR1b		400	0.45	2.25		
	PR2b		550	0.30	0.67		
	RR1b		315	0.60	1.17		
	RR2b		400	0.45	0.93		
	PR1c		400	0.45	2.25		
	PR2c		550	0.30	0.67		
	RR1c		315	0.60	1.17		
	RR2c		400	0.45	0.93		
	Sanchez		RR1i	mixed	314	0.61	1.25
			RR1ii	volcanics and	370	0.47	
RR1iii		chert (fine)	424	0.37			
RR2i		mixed	314	0.61			
RR2ii		volcanics and	370	0.77			
RR2iii		chert (coarse)	424	0.37			
Esposito	RR1	quartzite, quartz, (calcareous) chert, volcanic rock fragments (fine and coarse)	380	0.45	1.17		
	RR2	coarse grained quartz, quartzite, gneiss, metarhyolite (fine and coarse)					

Table 7: Overview of experimental tests in the literature: storage conditions.

Author	Pre-treatment				ASR development				
	Time d	Wrap.	Temp. °C	Moist.	Time d	Wrap.	Temp. °C	Moist.	
Swamy	No	No	No	No	365	No	20	96%	
Larive	11	Al-foil	23	98%	546	No	38	97%	
Monette	28	No	20	96%	147	No	38	1N NaOH solution	
Ahmed	28	No	20	in water	365	No	38	in water	
Multon	28	Al-foil	20	N/A	730	Al-foil	38	in box	
Ben Haha	a						20		
	b	No	No	No	No	365	No	40	in box on water
	c						60		
Giaccio	No	No	No	No	721/904	cotton	38	plastic bag with 5 ml water	
Sargolzahe	7	No	20	97%	700	No	38	in plastic box on water	
Giannini	No	No	No	No	120/270	No	38	95%	
Lindgård	a				365/784	No	38	in plastic box	
	b	1/7/28	No	20	in water (0.5hrs)	273	cotton	60	in metal box on water
	c				in water (0.5hrs)	365/273	cotton	38	in plastic box with lining
Sanchez	No	No	No	No	63/182	No	38	100%	
Esposito	No	No	No	No	365	No	38	96%	

Table 8: Overview of experimental tests in the literature: data name and corresponding marker in figures, asymptotic expansion and calculated reference values of the measured mechanical properties.

Author	Data set#		Expansion		Calculated reference value at $\varepsilon = 0.05\%$					
			Time d	$\varepsilon$	$E_{st}$ GPa	$E_{dyn}$ GPa	$f_c$ MPa	$f_{t,sp}$ MPa	MOR MPa	$f_{t,dir}$ MPa
Swamy	ER1	+	365	0.62	-	39.0	52.53	3.24	4.08	-
	ER2	×	365	1.64	-	34.3	43.08	-	-	-
Larive	RR	*	365	0.21 <sup>”</sup>	33.9	-	52.64	3.93	-	-
Monette	RR	×	147	0.35	18.8	38.2	27.51	-	5.87	-
Ahmed	RR	□ w	365	0.15	32.7	-	51.15	4.74	5.37	4.80
	ER1	□ g	365	0.73	36.3	-	50.30	5.05	6.76	2.60
	ER2	□ b	365	2.70	22.1 <sup>†</sup>	-	41.22 <sup>†</sup>	3.57 <sup>†</sup>	5.26 <sup>†</sup>	1.42 <sup>†</sup>
Multon	PR	+	365	0.10	32.6	-	42.01	3.14	-	-
Ben Haha	PR1ia	▽w	365	0.05	24.8	-	63.86	4.35	-	-
	PR1iia	▽g	365	0.07	24.8	-	51.43	3.81	-	-
	PR1iia	▽b	365	0.08	25.2	-	53.62	4.05	-	-
	PR1ib‡	△w	365	0.05	21.8	-	51.09	4.39	-	-
	PR1iib‡	△g	365	0.12	26.8	-	48.27	4.27	-	-
	PR1iib‡	△b	365	0.14	25.0	-	46.15	4.25	-	-
	PR1iic	◇g	365	0.14	25.0	-	46.15	4.25	-	-
	PR1iic	◇b	365	0.16	26.5	-	47.53	4.36	-	-
	PR2ia	▽w	365	0.05	26.4	-	34.26	4.25	-	-
	PR2iia	▽g	365	0.07	25.7	-	55.72	3.81	-	-
	PR2iia	▽b	365	0.07	24.9	-	54.73	3.93	-	-
	PR2ib‡	△w	365	0.12	26.7	-	50.47	4.22	-	-
	PR2iib‡	△g	365	0.14	26.0	-	48.98	4.33	-	-
	PR2iib‡	△b	365	0.14	25.8	-	47.93	4.25	-	-
	PR2iic	◇g	365	0.14	25.5	-	49.21	4.37	-	-
PR2iic	◇b	365	0.16	26.2	-	47.47	4.37	-	-	
Giaccio	PR	ow	365	0.08	38.1	-	36.50	-	-	-
	RR1	og	365	0.21	24.1 <sup>†</sup>	-	30.20 <sup>†</sup>	-	-	-
	RR2	ob	365	0.28	32.0	-	27.80	-	-	-
Sargolzahi	PR	*	365	0.08 <sup>”</sup>	32.5	20.9	43.02	-	-	-
Giannini	RR1	□ w	120	0.14	25.5	-	36.82	-	-	-
	RR2	□ b	270	0.42	25.4	-	34.52	-	-	-
Lindgård	PR1a‡	◁g	365	0.05	-	44.7	-	-	-	-
	PR2a‡	◁w	365	0.08	-	51.6	-	-	-	-
	RR1a‡	▷g	365	0.21	-	36.5	-	-	-	-
	RR2a‡	▷w	365	0.26	-	42.1	-	-	-	-
	PR1b	◁g	273	0.14	-	43.2	-	-	-	-
	PR2b	◁w	273	0.17	-	47.6	-	-	-	-
	RR1b	▷g	273	0.18	-	34.7	-	-	-	-
	RR2b	▷w	273	0.23	-	38.7	-	-	-	-
	PR1c	◁g	273	0.04	-	40.3 <sup>†</sup>	-	-	-	-
	PR2c	◁w	273	0.06	-	49.1	-	-	-	-
	RR1c	▷g	273	0.28	-	37.8	-	-	-	-
	RR2c	▷w	365	0.27	-	42.7	-	-	-	-
Sanchez	RR1i	ow	63	0.30	-	21.0	-	-	-	-
	RR1ii	og	63	0.30	-	29.5	-	-	-	-
	RR1iii	ob	63	0.30	-	28.0	-	-	-	-
	RR2i	ow	182	0.20	-	23.2	-	-	-	-
	RR2ii	og	182	0.20	-	30.9	-	-	-	-
	RR2iii	ob	182	0.20	-	29.3	-	-	-	-
Esposito	RR1	*b	365	0.11	39.5	-	60.11	3.76	-	-
	RR2	*g	365	0.18	26.1	-	61.23	3.85	-	-

‡ Sample used for the classification (for authors who tested the same mix in different storage conditions).

” Interpolated expansion value.

† Extrapolated value of the mechanical properties at the reference expansion. All the other data are interpolated.

# Data set and adopted marker in figures. If the symbol is repeated the size is decreased (e.g. Swamy-ER1 is identified with a larger + sign with respect to Multon-PR). The filler of the markers can be white (w), grey (g) or black (b).

Table 9: Fitting coefficients and standard deviation.

Data	S-curve					Piecewise linear curve					
	$\varepsilon_c$ %	$\varepsilon_l$ %	$\beta_0$	$\beta_\infty$	$\sigma$ %	$q_l$	$m_l$	$m_m$	$m_h$	$m_e$	$\sigma$ %
$E$	0.37	$1.13 \cdot 10^{-9}$	1.06	0.19	7	1.07	-1.06	-1.78	-0.98	-0.23	7
$E_{st}$	0.42	$2.27 \cdot 10^{-14}$	1.05	0.11	9	1.04	-0.46	-1.89	-1.08	-0.21	9
$E_{dyn}$	0.31	$6.89 \cdot 10^{-12}$	1.07	0.29	6	1.08	-1.43	-1.75	-0.91	-0.26	6
$f_c$	0.07	1.13	1.00	0.64	15	0.89	2.36	2.06	-0.37	-0.18	13
$f_t$	$5.24 \cdot 10^{-04}$	0.51	1.00	0.59	15	1.01	-0.15	0.20	-0.83	-0.08	15
$f_{t,sp}$	0.11	0.35	1.01	0.60	8	1.01	-0.25	-0.15	-0.86	-0.04	8
MOR	0.07	0.37	1.05	0.34	20	1.06	0.53	0.04	-1.54	-0.14	20
$f_{t,dir}$	0.10	2.15	1.05	0.70	12	0.97	2.23	-0.68	0.20	-0.18	13

521 **List of Figures**

522 1 Expansion behaviour (a) and deterioration of static elastic modulus (b), compress-  
523 ive strength (c) and splitting tensile strength (d) for the RR1 and RR2 concrete  
524 mixes. . . . . 32

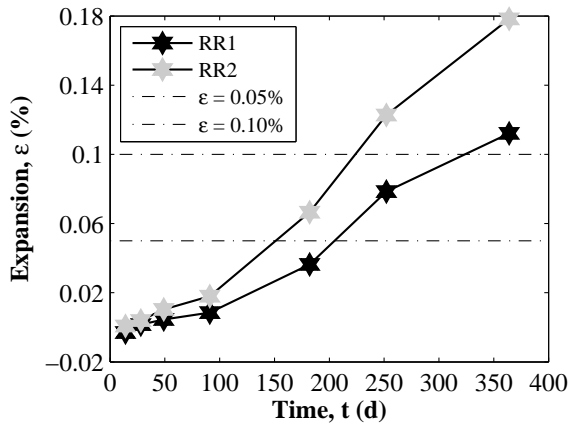
525 2 Experimental data from the literature: (a) Static elastic modulus; (b) Dynamic  
526 elastic modulus; (c) Compressive strength. A non-uniform scale for the expansion  
527 axis is used. For the legend see the description in Table 8. . . . . 33

528 3 Experimental data from literature: (a) Splitting tensile strength; (b) Modulus of  
529 rupture; (c) Direct tensile strength. A non-uniform scale for the expansion axis is  
530 used. For the legend see the description in Table 8. . . . . 34

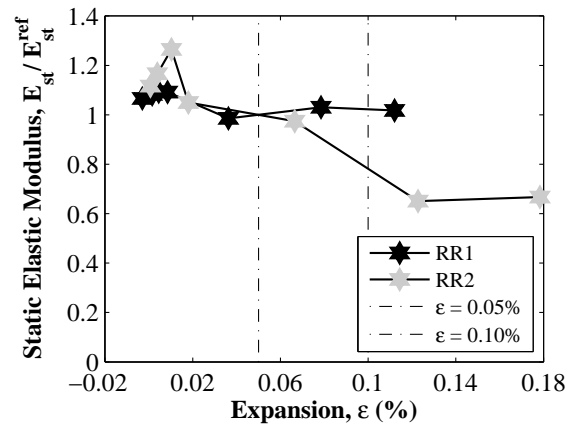
531 4 Fitting adopting S-shaped curve: (a) Elastic modulus; (b) Compressive strength;  
532 (c) Tensile strength. . . . . 35

533 5 Fitting adopting piecewise linear curve: (a) Elastic modulus; (b) Compressive  
534 strength; (c) Tensile strength. . . . . 36

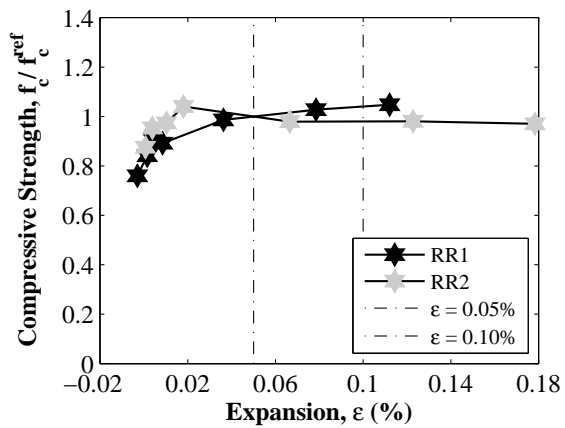
535 6 Best curve fitting results: (a) Relation between normalised properties and con-  
536 crete expansion; (b) Relation between normalised elastic modulus and normalised  
537 strengths. . . . . 37



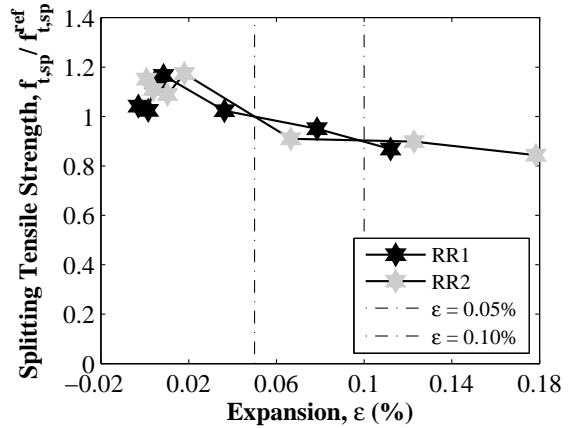
(a)



(b)

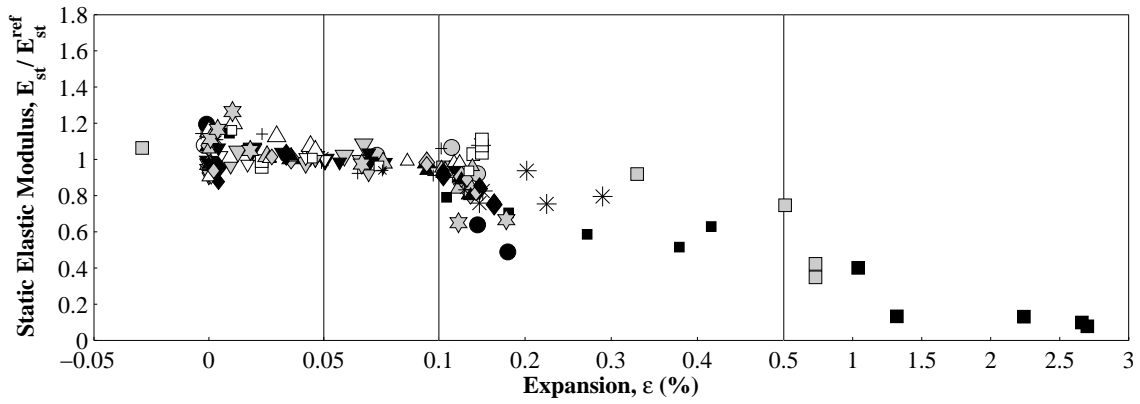


(c)

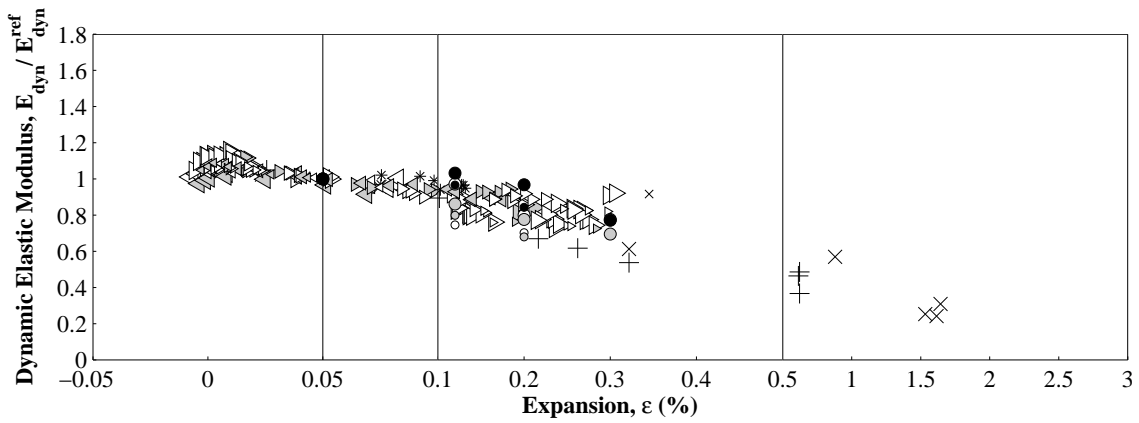


(d)

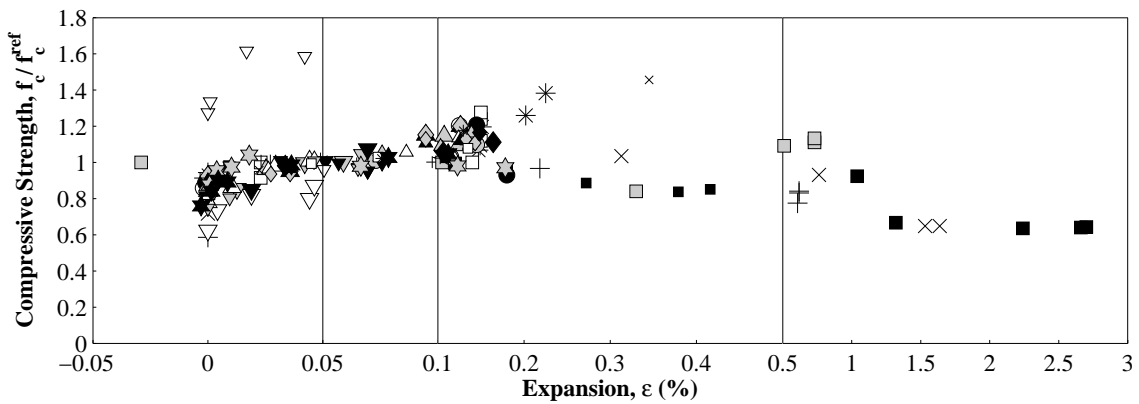
Figure 1: Expansion behaviour (a) and deterioration of static elastic modulus (b), compressive strength (c) and splitting tensile strength (d) for the RR1 and RR2 concrete mixes.



(a)

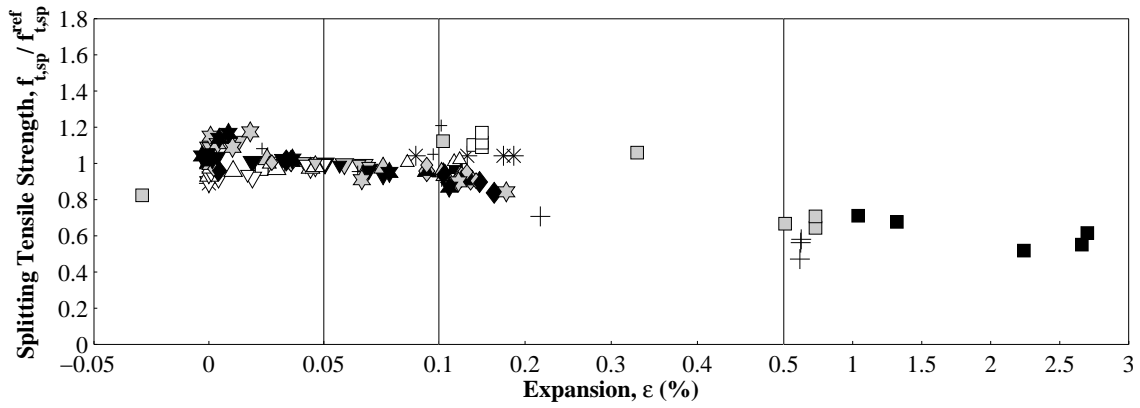


(b)

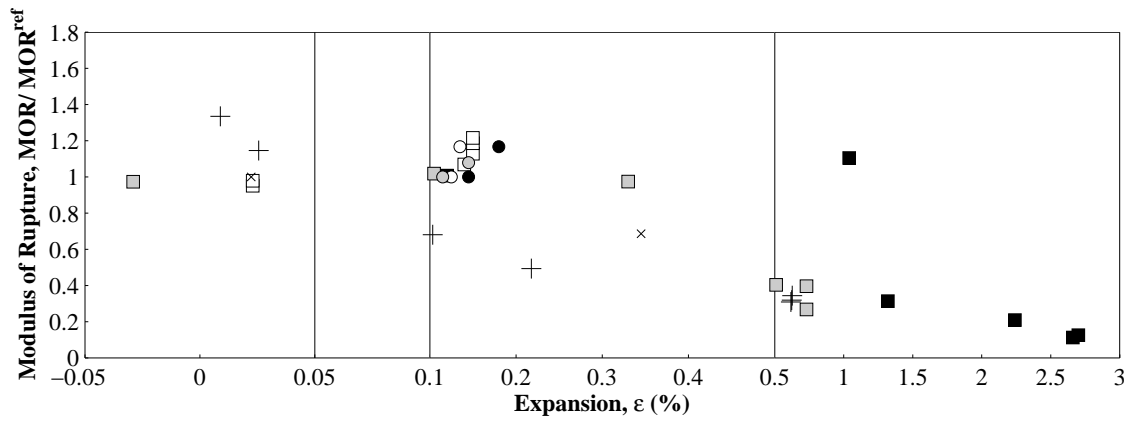


(c)

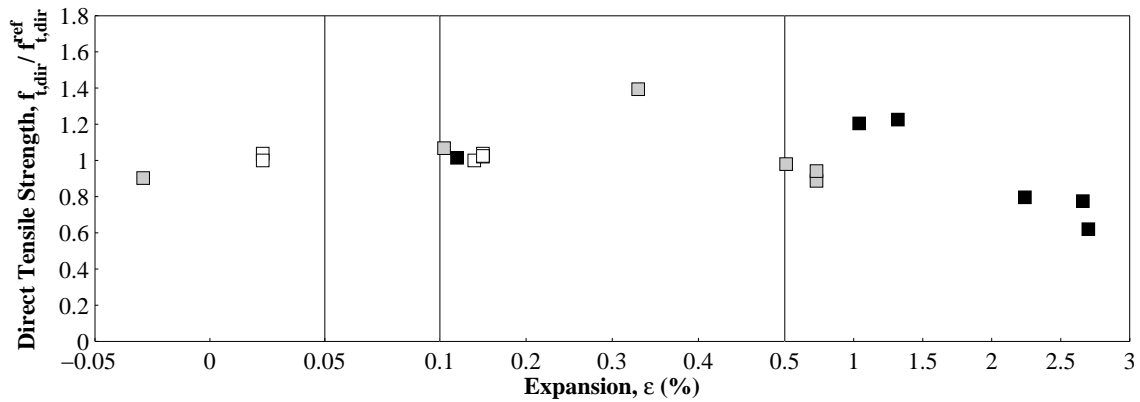
Figure 2: Experimental data from the literature: (a) Static elastic modulus; (b) Dynamic elastic modulus; (c) Compressive strength. A non-uniform scale for the expansion axis is used. For the legend see the description in Table 8.



(a)

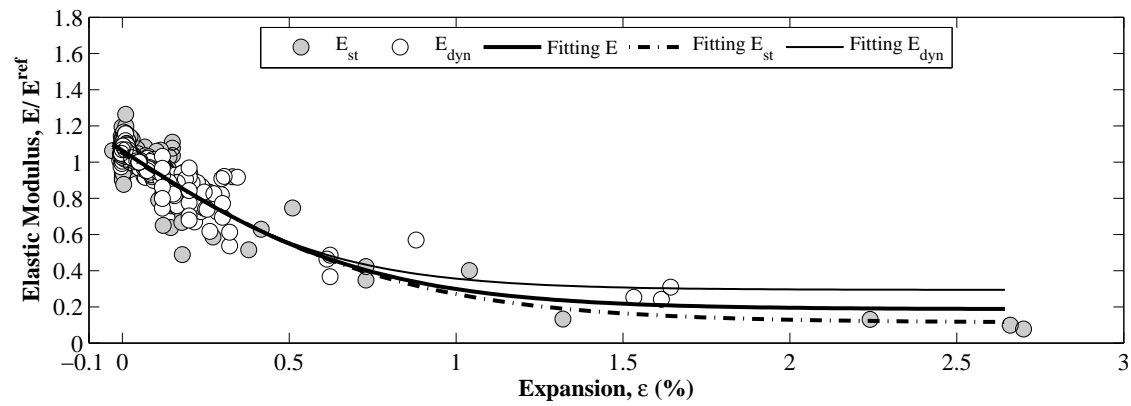


(b)

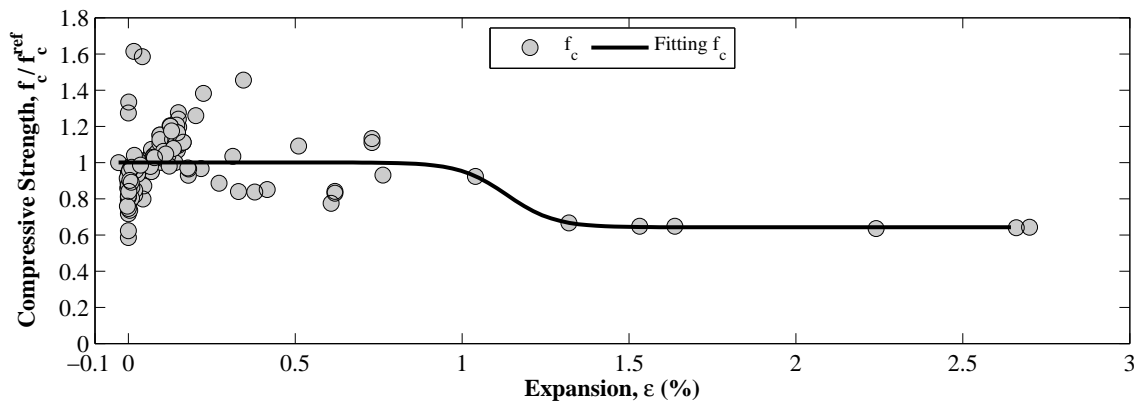


(c)

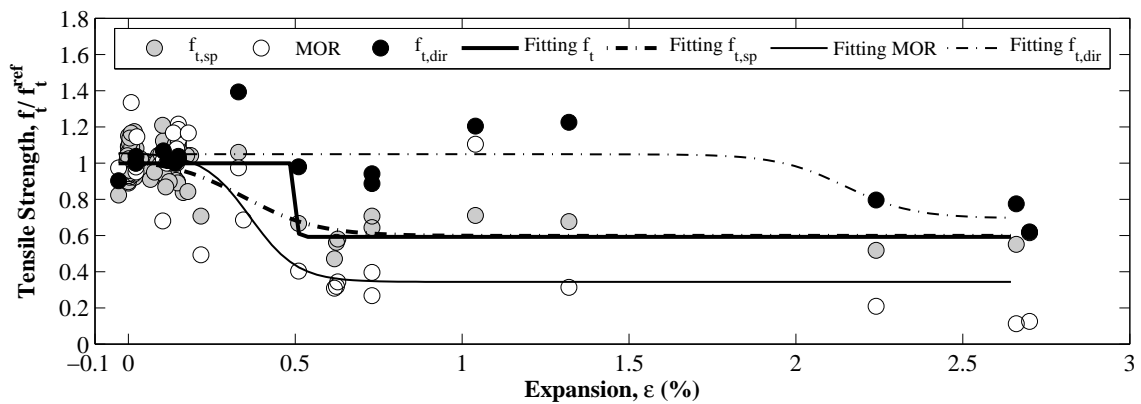
Figure 3: Experimental data from literature: (a) Splitting tensile strength; (b) Modulus of rupture; (c) Direct tensile strength. A non-uniform scale for the expansion axis is used. For the legend see the description in Table 8.



(a)

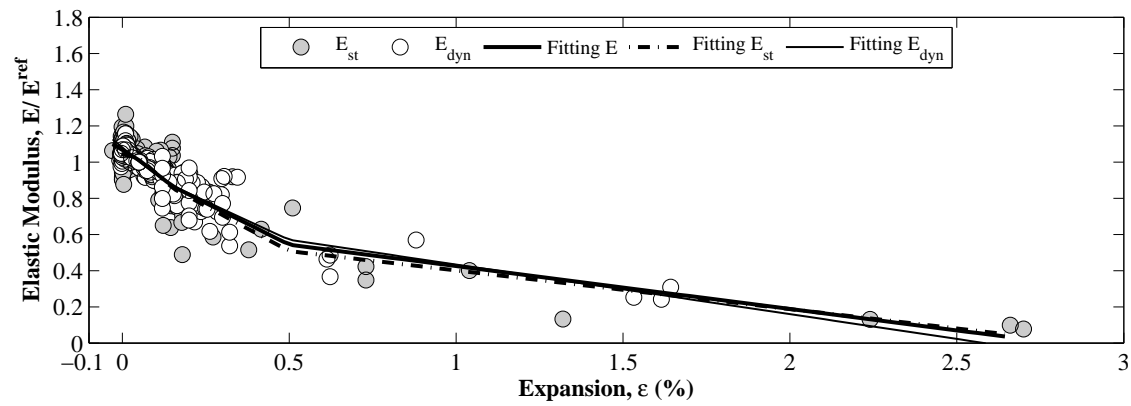


(b)

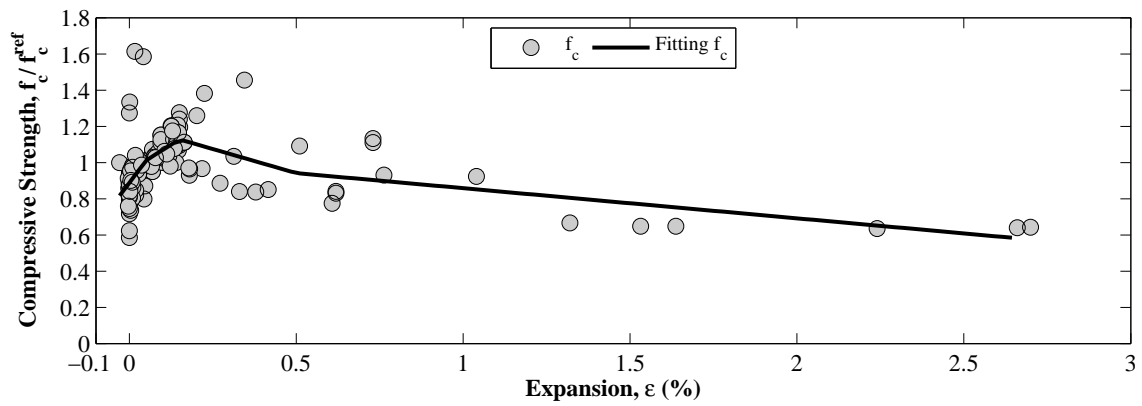


(c)

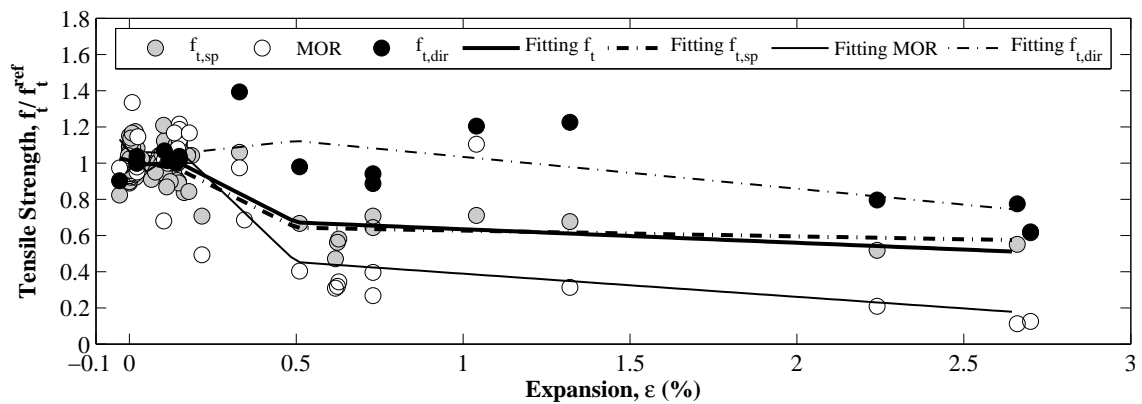
Figure 4: Fitting adopting S-shaped curve: (a) Elastic modulus; (b) Compressive strength; (c) Tensile strength.



(a)

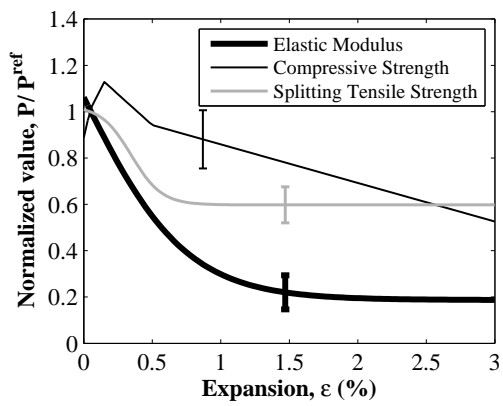


(b)

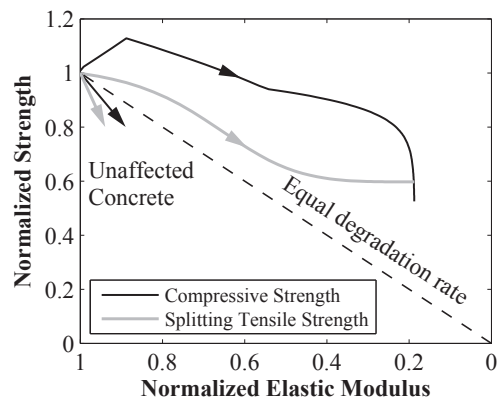


(c)

Figure 5: Fitting adopting piecewise linear curve: (a) Elastic modulus; (b) Compressive strength; (c) Tensile strength.



(a)



(b)

Figure 6: Best curve fitting results: (a) Relation between normalised properties and concrete expansion; (b) Relation between normalised elastic modulus and normalised strengths.